Real-Time Sensing Assisted Beam Selection for Communication on a 28 GHz ISAC Testbed

Juhyun Moon, Adam Dubs, and Sunwoo Kim
Department of Electronic Engineering, Hanyang University, South Korea
{juhn00, duanandi16, remero}@hanyang.ac.kr

Abstract

This paper implements and experimentally evaluates a beam selection scheme for mitigating beam misalignment in a 28 GHz ISAC testbed. The proposed approach utilizes a sensing session to determine the optimal communication beam. Specifically, it performs a beam sweep to measure received-power metrics and updates the communication beam-index pair by selecting the configuration that maximizes the received power. The selected beam-index information is fed back to the transmitter over a Wi-Fi link and applied to dynamically adjust the beam alignment. Using the constructed testbed, we compare link stability and transmission performance with and without beam adaptation, and demonstrate that the proposed scheme improves effective throughput.

***Index Terms*—Integrated sensing and communication, mmWave, beam adaptation, real-time testbed, analog beamforming**

I. Introduction

Integrated sensing and communication (ISAC) is becoming an essential element of next-generation wireless systems [1]. In high-frequency bands, notably mmWave, precise range and angle estimation can be achieved by leveraging wider bandwidths and beamforming. Nevertheless, signals in the mmWave band suffer from increased path loss and highly intermittent channels in the presence of common obstructions, limiting effective coverage and degrading link robustness [2]. Therefore, reliable ISAC requires beam management to enable directional beamforming through periodic beam sweeping and beam selection.

In this paper, we build a real-time ISAC testbed and implement a beam adaptation scheme in which the communication beam-index pair is updated at each transmission interval based on beam selection obtained during the sensing session, choosing the beam pair that maximizes the received power at the transmitter (TX) and receiver (RX). We present the testbed architecture and experimental procedure, and evaluate the proposed scheme in terms of effective throughput.

II. System Model

This paper considers a MIMO OFDM system, where the TX and RX each have N elements of uniform linear array (ULA), and the antenna element spacing of the ULA is the half-wavelength at the carrier frequency. An OFDM waveform with K subcarriers and a subcarrier spacing of Δf is employed. The received signal corresponding to the transmitted pilot signal $p_{\mu,\nu}$ can be expressed as

$$y_{\mu,\nu} = \mathbf{w}_{\mathrm{RX},i}^{\mathsf{H}} \mathbf{H}_{\mu,\nu} \mathbf{f}_{\mathrm{TX},j}^{*} p_{\mu,\nu} + n_{\mu,\nu}, \tag{1}$$

where $y_{\mu,\nu}$ denotes the received data at the μ-th symbol of the ν-th subcarrier, $\mathbf{w}_{\mathrm{RX},i}, \mathbf{f}_{\mathrm{TX},j} \in \mathbb{C}^{N\times 1}$ denote the i-th RX combiner and j-th TX precoder, respectively, and $n_{\mu,\nu}$ denotes the additive white Gaussian noise.

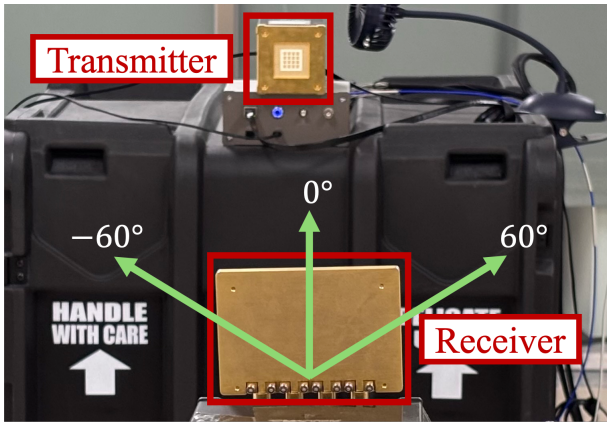

Fig. 1: Experimental setup for the mmWave link measurement.

The channel matrix $\mathbf{H}_{\mu,\nu} \in \mathbb{C}^{N\times N}$ consisting of L multi-path components (MPC) is expressed as

$$\mathbf{H}_{\mu,\nu} = \sum_{l=0}^{L-1} \alpha_{l,\mu,\nu} \mathbf{a}_{\mathrm{RX}}(\phi_l) \mathbf{a}_{\mathrm{TX}}(\theta_l)^{\top} e^{-\jmath 2\pi \tau_l \nu \Delta f}, \tag{2}$$

where $\mathbf{a}_{\mathrm{TX}}(\theta_l), \mathbf{a}_{\mathrm{RX}}(\phi_l) \in \mathbb{C}^{N\times 1}$ denote the steering vectors at the TX and RX, $\alpha_{l,\mu,\nu}, \phi_l, \theta_l$ and τ_l denote the complex gain, the AoA, the AoD, and the propagation delay of the l-th path respectively. Here, $\jmath$ denotes the imaginary unit.

III. Beam Selection And Feedback Protocol

We implement a beam selection and feedback protocol that maintains beam alignment by periodically performing a sensing-session beam sweep and using the sensing outcome to update the communication beam-index pair based on received-power measurements. In each update interval, the receiver performs a codebook-based sensing-beam sweep and acquires pilot-based measurements for all candidate beam pairs (i, j), from which the beamformed channel frequency response (CFR) is obtained. Specifically, for the μ-th OFDM symbol

TABLE I: OFDM WAVEFORM AND BEAM SWEEP SPECIFICATIONS

Parameters	Value
Center frequency	28 GHz
Bandwidth	Sens. – 1.92 GHz, Comm. – 43.2 MHz
# of subcarriers	Sens. – 4000 / Comm. – 90 (@bin: 480 kHz)
Antenna size	Tx: 16(4×4); Rx: 16(4×4)
Tx beamsweep range	$-60°$ to $60°$ (@$5°$ intervals)
Rx beamsweep range	$-60°$ to $60°$ (@$5°$ intervals)

and the ν-th subcarrier, the CFR estimate for beam pair (i, j) is given by

$$\hat{h}_\nu(i,j) = \frac{y_{\mu,\nu}}{p_{\mu,\nu}} = \mathbf{w}_{\mathrm{RX},i}^{\mathsf{H}} \mathbf{H}_{\mu,\nu} \mathbf{f}_{\mathrm{TX},j}^{*} + \tilde{n}_{\mu,\nu}, \tag{3}$$

where $\tilde{n}_{\mu,\nu}$ denotes the effective noise. The subcarrier-domain CFR is transformed into the delay-domain Channel Impulse Response (CIR) as

$$h_{i,j}[\tau] = \frac{1}{K} \sum_{\nu=0}^{K-1} \hat{h}_\nu(i,j) e^{j\frac{2\pi\nu\tau}{K}}, \tag{4}$$

where $\tau \in \{0, \cdots, K-1\}$ denotes the delay index. Subsequently, the power-delay profile for beam pair (i, j) is expressed as

$$P_{i,j}[\tau] = |h_{i,j}[\tau]|^2. \tag{5}$$

Accordingly, the beam-index pair (i^*, j^*) to be applied in the next update interval is determined by

$$(i^*, j^*) = \arg\max_{i\in\mathcal{I}, j\in\mathcal{J}} (\max_{\tau} P_{i,j}[\tau]), \tag{6}$$

where $\mathcal{I}$ and $\mathcal{J}$ denote the predefined RX and TX beam codebooks, respectively. The selected (i^*, j^*) is recorded as the beam decision and used to update the receiver beam. For the update procedure, the RX applies (i^*, j^*) to the hardware control interface for the next interval. Simultaneously, the decision is fed back to the TX via a Wi-Fi UDP link to be synchronized and applied in the subsequent interval.

IV. Experimental Results

A. Hardware Configuration and Experimental Setup

The experiment was conducted on an ISAC testbed built on National Instruments' mmWave Transceiver System (MTS) with TMYTEK's BBox uniform rectangular array (URA) antennas [3], [4]. One-way transmission used separate PXIe-8880 chassis for the TX and RX. Following the specification in Table I, pilot reference symbols were transmitted over 625 consecutive symbols by sweeping 625 TX–RX beam pairs formed from 25 TX and 25 RX beam directions to sample the FOV at both ends. Oven-controlled crystal oscillator (OCXO) clocks and an over-the-air signaling mechanism were used for data acquisition triggering and synchronization [5]. With the receiver kept fixed, the transmitter was placed 1.82 m away and positioned at $-60°$, $-30°$, $0°$, $30°$, and $60°$ relative to the receiver, dwelling for 25s at each angle while measurements were collected. The same measurement procedure was repeated with and without beam adaptation.

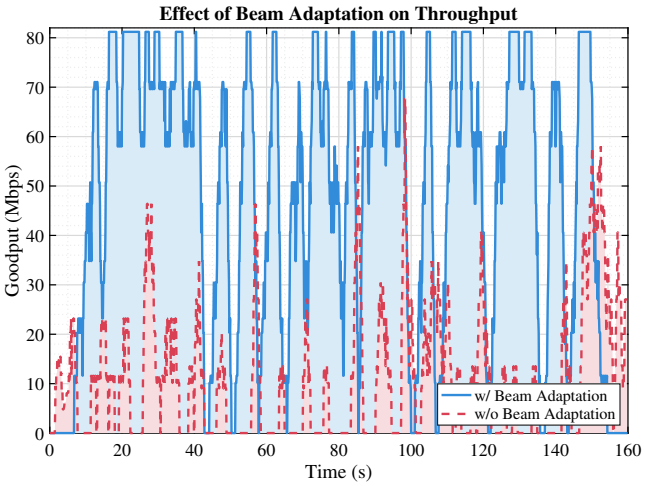

Fig. 2: Effective throughput with/without beam adaptation.

B. Experimental Results

Effective throughput was evaluated from CRC outcomes and smoothed using a sliding-window average ($W = 1.5$s), as shown in Fig. 2. Beam adaptation provides a substantial improvement: the average effective throughput increases from 11.36 Mbps without adaptation to 47.32 Mbps with adaptation, and the delivered data volume over the approximately 160s interval increases from 226.72 MB to 946.23 MB. These results indicate that beam adaptation significantly enhances end-to-end data delivery under angular variation by maintaining higher effective throughput over time.

V. Conclusions

In this paper, we developed a real-time mmWave ISAC testbed and implemented a beam adaptation scheme that selects the TX–RX beam pair maximizing the received power, with feedback delivered via a Wi-Fi link. Experimental results confirm that beam adaptation significantly improves effective throughput under angular variation. These findings highlight that beam adaptation enhances link robustness and end-to-end data delivery by maintaining beam alignment over time.

Acknowledgment

The fundamental research described in this paper was supported by the National Research Foundation of Korea under Grant RS-2024-00409492.

References

[1] F. Liu, Y. Cui, C. Masouros, J. Xu, T. X. Han, Y. C. Eldar, and S. Buzzi, "Integrated sensing and communications: Toward dual-functional wireless networks for 6g and beyond," *IEEE J. Sel. Areas Commun.*, vol. 40, pp. 1728–1767, Jun. 2022.

[2] M. Giordani, M. Polese, A. Roy, D. Castor, and M. Zorzi, "A tutorial on beam management for 3gpp nr at mmwave frequencies," *IEEE Communications Surveys & Tutorials*, vol. 21, no. 1, pp. 173–196, 2019.

[3] *mmWave Transceiver System Getting Started*, National Instruments, February 2023. [Online]. Available: https://www.ni.com/docs/en-US/bundle/mmwave-transceiver-system-getting-started/page/overview.html

[4] *Datasheet BBox One 5G 28 GHz BNE-2840-G*, TMYTEK, October 2022. [Online]. Available: https://tmytek.com/resources/documents

[5] *PXIe-6674T Specifications*, National Instruments, June 2023. [Online]. Available: https://www.ni.com/docs/en-US/bundle/pxie-6674t-specs/page/specs.html